Journal of The Electrochemical Society, **156** (5) H320-H326 (2009)
0013-4651/2009/156(5)/H320/7/$23.00 © The Electrochemical Society

Effects of Counteranions and Dissolved Oxygen on Chemical ZnO Deposition from Aqueous Solutions

Tsutomu Shinagawa,[a,z] Kuniaki Murase,[b,*] Satomi Otomo,[c] Jun-ichi Katayama,[c] and Masanobu Izaki[d,*]

[a]*Electronic Materials Research Division, Osaka Municipal Technical Research Institute, Osaka 536-8553, Japan*
[b]*Department of Material Science and Engineering, Kyoto University, Kyoto 606-8501, Japan*
[c]*Okuno Chemical Industries Company, Limited, Basic Research Laboratory, Osaka 538-0044, Japan*
[d]*Department of Production System Engineering, Toyohashi University of Technology, Toyohashi 441-8580, Japan*

In the chemical ZnO deposition on Pd-catalyzed glass from aqueous dimethylamineborane (DMAB) solutions, effects of counteranions (NO_3^-, Cl^-, ClO_4^-, and SO_4^{2-}) and dissolved oxygen (DO) on the hydrolysis behavior of Zn^{2+} and the growth regime of ZnO were studied using sodium and zinc salt solutions bubbled with O_2, air, or Ar gas. The interaction of the counteranions with H^+ and Pd as well as Zn^{2+} was suggested as an important factor for the chemical ZnO deposition, and it was found that only NO_3^- can raise the pH of a DMAB solution without DO, affording the continuous ZnO growth. Dissolved oxygen accelerated the ZnO nucleation process on the Pd and had less influence comparable to NO_3^- on the subsequent growth on the ZnO surface. The ZnO films deposited from $Zn(NO_3)_2$–DMAB solutions bubbled with O_2, air, or Ar gas were characterized with an X-ray diffractometer, field emission scanning electron microscope, UV-visible spectrophotometer, and Hall coefficient analyzer. The Ar-bubbled solution gave superior ZnO films in terms of crystallinity, growth orientation, surface morphology, and electrical conductivity due to the relatively moderate crystal nucleation compared to in the presence of DO.
 [DOI: 10.1149/1.3089353]

Manuscript submitted November 10, 2008; revised manuscript received February 2, 2009. Published March 11, 2009.

Zinc oxide (ZnO) is an n-type II-VI semiconducting oxide with a bandgap energy of 3.3 eV, which makes it transparent to visible light, and is widely used in industrial applications, such as varistors, chemical gas sensors, and surface acoustic wave devices, due to its various useful properties of semiconductivity, piezoelectricity, fluorescence, and photoconductivity.[1-4] In addition, ZnO has received much attention as a transparent conductive oxide[5] and a UV light-emitting material.[6-8] Recent vigorous developments in optoelectronic devices, such as flat-panel displays, have heightened the demand for low-cost transparent conductive films. Because zinc is an inexpensive common metal element, ZnO is a promising candidate for alternatives to indium tin oxide, consisting of a quite expensive rare-metal element.

As one of the nonvacuum and low-temperature soft processes, the formation of a polycrystalline wurtzite ZnO film from aqueous $Zn(NO_3)_2$ and $ZnCl_2$ solutions using an electrochemical method has been reported by Izaki and Omi,[9-11] and Peulon and Lincot,[12,13] respectively. The scheme of both the deposition methods is based on a local-pH increase in the vicinity of an electrode, resulting in precipitation by the hydrolysis of Zn^{2+} at around pH 6 [14]

$$Zn^{2+} + 2OH^- \rightarrow ZnO + H_2O \quad [1]$$

It was reported that, in the case of $Zn(NO_3)_2$ solution, the cathodic reduction of NO_3^- ions

$$NO_3^- + H_2O + 2e^- \rightarrow NO_2^- + 2OH^- \quad E^0 = 0.01 \text{ V vs NHE} \quad [2]$$

is a key to raising the pH, where NHE is the normal hydrogen electrode.[10] In contrast, the cathodic reduction of dissolved oxygen (DO)

$$O_2 + 2H_2O + 4e^- \rightarrow 4OH^- \quad E^0 = 0.401 \text{ V vs NHE} \quad [3]$$

is another key reaction in the case of NO_3^- ion-free, for example, $ZnCl_2$ and $ZnSO_4$ solutions. In the above electrochemical process, electrical conductivity is obviously required for the substrate. In contrast, chemical (electroless) deposition of ZnO on a nonconductive substrate, including glass and polymer, was achieved by Izaki and Omi[15] and Izaki and Katayama[16] using an aqueous $Zn(NO_3)_2$–dimethylamineborane (DMAB) solution. In this case, oxidation of DMAB is catalyzed by palladium nanoparticles decorated on the nonconductive substrate

$$(CH_3)_2NHBH_3 + H_2O \xrightarrow{Pd} HBO_2 + (CH_3)_2NH_2^+ + 5H^+ + 6e^- \quad [4]$$

and the electrons released by this reaction are used for Reaction 2, resulting in the deposition of ZnO. It should be noted that although DMAB releases five protons that decrease the pH, the six electrons released give six hydroxide ions via Reaction 2, resulting in the net reaction with one hydroxide ion generation. Furthermore, HBO_2 and $(CH_3)_2NH_2^+$ generated from DMAB, which have acid dissociation constants, pK_a, of 9.24 [17] and 10.77,[18] respectively, can release few protons below pH 8. This means that the pH in the vicinity of the Pd-catalyzed substrate can readily be raised up to pH 8. The Pd-catalyzed substrate can be prepared by a simple dipping process using three aqueous solutions;[19] hence, this chemical solution process without an external power source is suitable for fabricating large-area ZnO films onto nonconductive substrates at lower cost. Because DMAB is a relatively moderate reductant, the reversible acid-base Reaction 1 proceeds under near equilibrium condition (i.e., under weak driving force). Such a condition, therefore, leads to the deposition of ZnO with a larger grain size and inhibits the rapid decomposition of the bulk solution.

When an aqueous $Zn(NO_3)_2$−DMAB solution is employed to deposit ZnO without deaeration, (i.e., in the presence of ambient dissolved oxygen), the electrons released by Reaction 4 can also be consumed by Reaction 3. Therefore, not only Reaction 2 but also Reaction 3 can increase the local pH. According to our in situ investigation of the ZnO deposition using an electrochemical quartz crystal microbalance with gold coating, we found some sign that DO more or less works in the initial stage of ZnO growth, while nitrate ions seem to play an important role as a counteranion of Zn^{2+} as well as a precursor of OH^- ions.[20] In the electrochemical route, ZnO has been yielded from different zinc salts as mentioned above, and the effect of their counteranions on the ZnO growth was reported recently.[21] Even though the counteranion is one of the major components in the deposition solution, little has been investigated in the chemical (electroless) route. Furthermore, the detailed role of DO on the chemical ZnO deposition using a conventional Pd-catalyzed

* Electrochemical Society Active Member.
z E-mail: tshina@omtri.city.osaka.jp

glass substrate was still unclear. In the present study, we have therefore looked deeper into the effect of counteranions (NO_3^-, Cl^-, ClO_4^-, and SO_4^{2-}) and DO on the hydrolysis behavior of Zn^{2+} and the growth regime of ZnO. Significant differences based on the chemical nature of these counteranions were observed, and the negative influence of DO on the resulting ZnO was revealed.

Experimental

General procedures.— Chemical deposition of ZnO films from aqueous solutions was carried out using reagent-grade chemicals and deionized (DI) water purified by a Milli-RX12 Plus system. A Corning glass (no. 1737, 20 × 40 × 0.7 mm) was used as a substrate. Prior to each chemical deposition, the substrate was rinsed with acetone and DI water and was activated using a commercialized three-step Sn/Ag/Pd dipping process (Okuno Chemical Industries, Techno Clear series). This activation process comprises a sequential immersion of the substrate into the three solutions for 1 min each, resulting in the substrate being entirely covered with Pd nanoparticles at a high density.

pH variation of aqueous solutions.— An aliquot of DI water (0.15 dm^3) was placed in an airtight glass vessel, and a sodium or zinc salt with counteranions (NO_3^-, Cl^-, ClO_4^-, or SO_4^{2-}) was added so that the resulting solution contained 0.12 M of the counteranion in question (M = mole per cubic decimeter). The pH of the solutions was roughly adjusted to 4 with a corresponding hydroacid or oxoacid solution. A conventional glass electrode or an ion-sensitive field-effect transistor electrode was used for the pH measurement. The resulting solution was bubbled with O_2, air, or Ar gas for 1.5 h and DMAB was added so that the concentration was 0.02 M; the bubbling was continued until the end of the experiment. The pH was then readjusted to 4.17 with the corresponding acid solution. After 10 min from the DMAB addition, a Pd-catalyzed glass substrate was immersed in the solution and the pH variation was measured at 298 K with magnetic stirring and bubbling.

Chemical deposition of ZnO.— In a similar manner to the above, one of the zinc salts and DMAB were dissolved into DI water (0.15 dm^3) bubbled with O_2, air, or Ar gas for 1.5 h in advance to prepare an aqueous 0.06 M zinc salt−0.02 M DMAB solution. The resulting solution in an airtight vessel was heated to 338 K, and then a Pd-catalyzed glass substrate was immersed into the solution to deposit ZnO without stirring. During the deposition, the gas was passed into the free space of the vessel instead of the bubbling. The film obtained was rinsed with DI water and dried under ambient atmosphere. For Hall coefficient measurements, ZnO films were heat-treated in advance at 723 K for 30 min under a 3% H_2/Ar mixed gas atmosphere.

Characterization of ZnO.— X-ray diffraction (XRD) patterns were measured using a Rigaku RINT2500 system with monochromated Cu Kα radiation (40 kV, 200 mA). The thickness of films was measured at three different positions by a stylus profiler (Kosaka Lab., Surfcorder ET3000i), and the three measured values were averaged. Micromorphology of films was observed with a field emission scanning electron microscope [(FESEM), JEOL, JSM-6700F]. Optical transmittance spectra were recorded with a UV-visible spectrophotometer (Shimadzu, UV-3150C) with respect to air. The bandgap energy of ZnO was estimated by extrapolating the linear part of the relationship between α^2 and photon energy to $\alpha^2 = 0$, where α is the absorption coefficient. Electrical properties, including resistivity and carrier type, were evaluated with a van der Pauw method using a Hall coefficient analyzer (Toyo Technica, Resitest 8310).

Results and Discussion

Figure 1 shows a potential-pH diagram of the Zn–H_2O system, calculated using a set of thermochemical data cited in the paper by Goux et al.[22] Here, the activity of Zn^{2+} ($a_{Zn^{2+}}$) was set at 0.06,

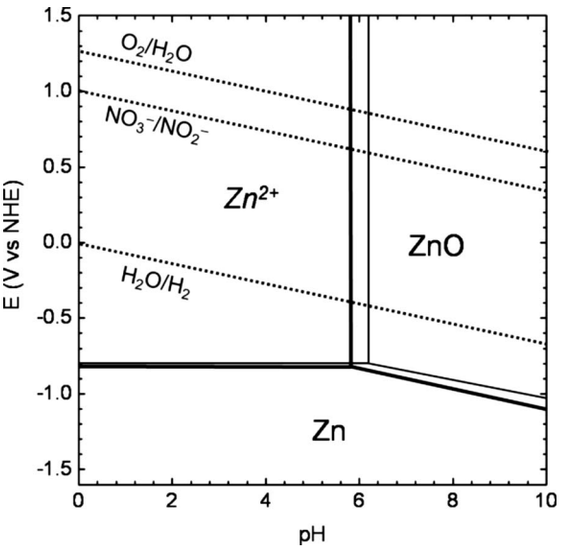

Figure 1. Potential-pH diagram of the Zn–H_2O system (thick line: 338 K, thin line: 298 K, $a_{Zn^{2+}} = 0.06$). Redox potentials for Reactions 2 and 3 at 338 K are also indicated ($a_{NO_3^-} = 0.12$, $a_{NO_2^-} = 10^{-6}$, $p_{O_2} = 1$, $p_{H_2} = 1$ atm).

which corresponds approximately to the present ZnO deposition condition, 0.06 M Zn^{2+}. The boundary pH between Zn^{2+} and ZnO (Reaction 1) is 6.2 at 298 K and 5.8 at 338 K. Because the initial pH of the 0.06 M $Zn(NO_3)_2$–0.02 M DMAB solution was 6.0 at 298 K, spontaneous hydrolysis of Zn^{2+} ions is thermodynamically supposed to take place at 338 K, if the pH is kept constant through the heating. However, the fact is that the initial solution was stable and no precipitation was recognized at 338 K for over 3 h in the absence of a Pd-catalyzed glass substrate under ambient atmosphere, suggesting that the solution was in a supersaturated state of, for example, dissolved $Zn(OH)_x$ species. Therefore, a local pH increase in the vicinity of a Pd-catalyzed glass substrate via the redox reactions (Reactions 2-4) can be a trigger to deposit ZnO on the glass without precipitation in the bulk solution.

Effect of counteranions on pH increase.— To examine the effect of the counteranions on the pH increase induced by the DMAB oxidation (Reaction 4) and subsequent dissolved oxygen reduction (Reaction 3), oxygenated aqueous 0.02 M DMAB solutions containing a sodium salt of major strong acids (i.e., $NaNO_3$, NaCl, $NaClO_4$, or Na_2SO_4) were prepared in such a way that the concentration of the counteranion was 0.12 M. The pH of each solution was adjusted to 4.17, and then a Pd-catalyzed glass substrate was immersed into the solution at 298 K with continuous magnetic stirring. The pH variation of the bulk solution after the immersion is given in Fig. 2a and the apparent generation rate of OH^- calculated from the early-stage pH variation is in Table I. Here, the data recorded for a sodium salt-free solution are included for reference. The pH of the aqueous solution containing NO_3^- or ClO_4^- as a counteranion increased readily like a neutralizing titration curve of an acidic solution. This trend is similar to that of the sodium salt-free solution, indicating that these counteranions have little influence on the redox reactions (Reactions 3 and 4) causing a pH increase. Actually, the OH^--generation rate for the NO_3^- solution was calculated to be 6.1 μmol min^{-1}; the highest among them. The rapid pH increase was then buffered at pH over 8 by HBO_2 ($pK_a = 9.24$) generated from DMAB (Reaction 4), as mentioned above and also demonstrated in Fig. 2c. In contrast, the addition of Cl^- or SO_4^{2-} ion inhibited a rapid pH increase. The pH increase rate of the solution containing SO_4^{2-} was $<1/10$ that of the NO_3^- solution, and pH was 8.8 even after 2 h. The exact reason for the difference in pH increase is still unclear at this time. We, however, have an impression that the

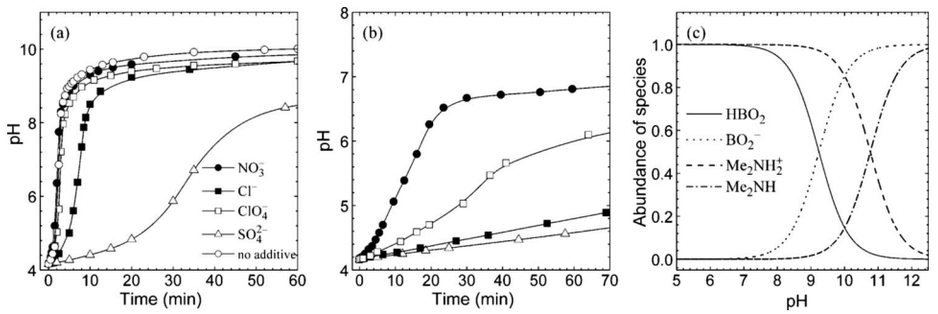

Figure 2. pH variations under continuous O_2 bubbling at 298 K after the immersion of Pd-catalyzed glass into aqueous 0.02 M DMAB solutions containing (a) sodium salts or (b) zinc salts: NO_3^- (●), Cl^- (■), ClO_4^- (□), SO_4^{2-} (△), no additive (○). For each run, the concentration of the counteranion is 0.12 M, and the initial pH is adjusted to 4.17. (c) Calculated abundance of dissolved chemical species generated by the oxidation of DMAB.

behavior is related to the strength of anion as a Lewis base. The acid dissociation constant for HNO_3 is −1.43 (=pK_a), while that for HSO_4^- is 1.99,[23] suggesting that SO_4^{2-} ions have relatively stronger coordination ability toward H^+, Na^+, and some other species in the solution. This might affect the rate of Reaction 3 or 4. Alternatively, SO_4^{2-} ions adsorbed to the surface of the Pd particles can inhibit the decomposition of DMAB.[24] The relatively slow pH increase for Cl^- solution compared to the case of NO_3^- and ClO_4^- ions may also be accounted for by such catalyst poisoning through the interaction between Cl^- ions and the Pd surface.[25]

Similar experiments recording a pH variation of aqueous DMAB solutions were carried out by using corresponding zinc salts instead of sodium ones (Fig. 2b). Although in these cases the pH increase of the solutions is strongly buffered by Zn^{2+}/ZnO or $Zn^{2+}/Zn(OH)_2$ acid-base reaction at around pH 6.2, the counteranion-dependent pH increase is clearly observed: the NO_3^- solution showed the fastest pH increase rate, and that of the solution containing Cl^- or SO_4^{2-} ion was found very low (see also Table I). These noticeable differences in pH increase in terms of counteranions are attributed to their multiple interactions with H^+, Zn^{2+} ions, and the Pd catalyst, as discussed in the next section. Note that such slow pH increase does not necessarily follow the inability of ZnO deposition because the net OH^- ions required for the ZnO generation in the vicinity of a substrate, not in the bulk solution, is quite small.

Effect of counteranions on ZnO growth.— The influence of the multiple interactions between the counteranion and H^+, Zn^{2+} ions, and the Pd catalyst on the ZnO growth under a typical deposition condition was examined using the same series of oxygenated solutions containing the zinc salts. Figure 3 shows XRD patterns of the deposits obtained by immersing a Pd-catalyzed glass substrate for 1 h at 338 K. Wurtzite ZnO was obtained only from the solution containing a NO_3^- or ClO_4^- ion. Deposits obtained from the Cl^- and SO_4^{2-} solutions had XRD peaks at 2θ of 11.2 and 8.0°, respectively, and they were identified as $Zn_5Cl_2(OH)_8 \cdot H_2O$ (JCPDS no. 07-0155) and $Zn_4(SO_4)(OH)_6 \cdot 5H_2O$ (JCPDS no. 39-0688). It is thought that, because Cl^- and SO_4^{2-} ions have relatively high stability constants with Zn^{2+} ($Zn^{2+} + Cl^- = ZnCl^+$, $\log K_{Cl^-} = 0.11$; $Zn^{2+} + SO_4^{2-} = ZnSO_4$, $\log K_{SO_4^{2-}} = 0.89$),[23] such double salt hydrates are liable to form in the neutral pH region. Even in the case of Cl^- and SO_4^{2-} solutions, ZnO could be formed if the pH increased to a higher level. In fact, ZnO have successfully been obtained by an electrochemical method from aqueous $ZnCl_2$ and $ZnSO_4$ solutions, where an external power source forcibly supplies a cathodic current to a substrate.[12,21] In the present case, however, the moderate hydrolysis

Table I. Apparent generation rate of OH^- ions in aqueous 0.02 M DMAB solutions with Pd-catalyzed glass and various salts. These values were calculated from Fig. 2a and b, 4, and 5.

Additives		OH^- generation rate (μmol/min)	
Anion	Cation	O_2 bubbling	Ar bubbling
NO_3^-	Na^+	6.1	0.21
	Zn^{2+}	1.1	0.27
Cl^-	Na^+	1.7	
	Zn^{2+}	0.18	
ClO_4^-	Na^+	4.4	0.15
	Zn^{2+}	0.41	
SO_4^{2-}	Na^+	0.46	
	Zn^{2+}	0.16	
No additive		4.1	0.14
No additive			0.085[a]

[a] Without Pd-catalyzed glass.

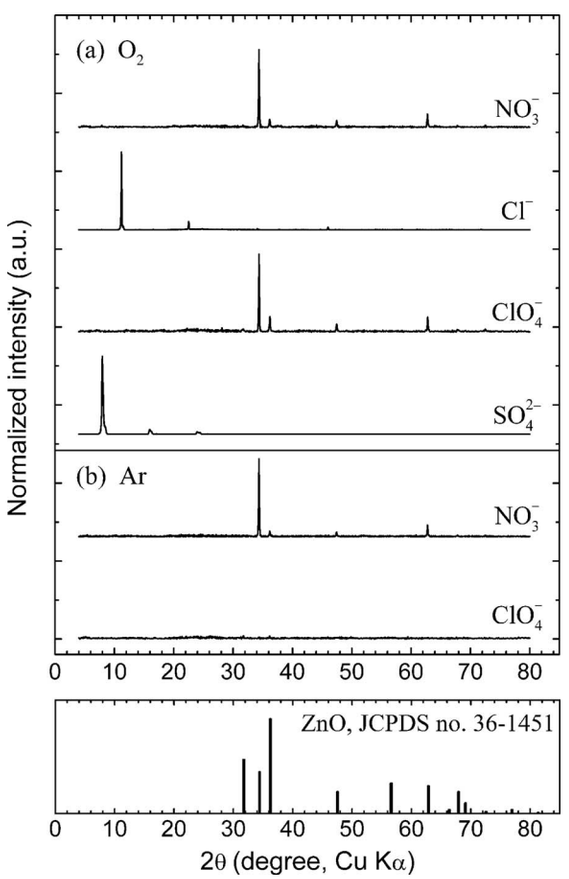

Figure 3. Normalized XRD patterns of deposits obtained by immersing Pd-catalyzed glass into (a) O_2- or (b) Ar-bubbled aqueous 0.06 M zinc salts–0.02 M DMAB solutions for 1 h at 338 K. JCPDS (no. 36-1451) data of wurtzite ZnO is also indicated.

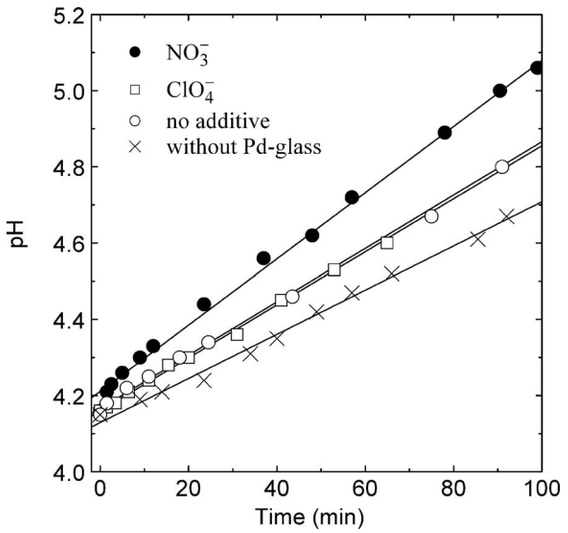

Figure 4. pH variations under continuous Ar bubbling at 298 K after the immersion of Pd-catalyzed glass into aqueous 0.02 M DMAB solutions containing sodium salts: NO_3^- (●), ClO_4^- (■), no additive (○), no additive and without the glass immersion (×). For each run, the concentration of the counteranion is 0.12 M, and the initial pH is adjusted to 4.17.

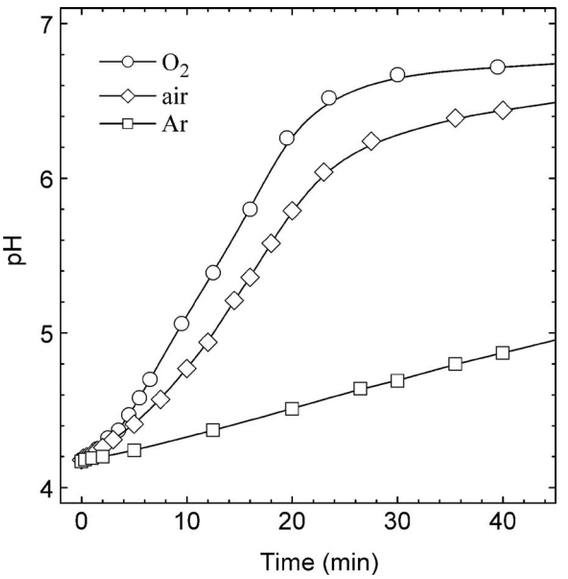

Figure 5. pH variations at 298 K after the immersion of Pd-catalyzed glass into aqueous 0.06 M $Zn(NO_3)_2$–0.02 M DMAB solutions with continuous O_2 (○), air (◇), or Ar (□) gas bubbling. For each run, the initial pH is adjusted at 4.17.

condition leads to the deposition of the double salt hydrates on the glass in preference to ZnO or $Zn(OH)_2$. In consequence, a counteranion having low stability constants with a Zn^{2+} ion such as NO_3^- ($Zn^{2+} + NO_3^- = ZnNO_3^+$, $\log K_{NO_3^-} = -0.2$)[17] and ClO_4^- ions is indispensable for the chemical (electroless) ZnO deposition from the DMAB solutions. (Note that, as well-known among electrochemists, the interaction between ClO_4^- anions and metal cations is negligible, while the $\log K_{ClO_4^-}$ for the reaction $Zn^{2+} + ClO_4^- = ZnClO_4^-$ is not reported.)

The reduction of NO_3^- ions gives OH^- ions through Reaction 2, as mentioned above. Similarly, it is thermodynamically possible that ClO_4^- ions are reduced to yield OH^- ions, while the redox potential is nobler than that of NO_3^-

$$ClO_4^- + H_2O + 2e^- \rightarrow ClO_3^- + 2OH^- \quad E^0 = 0.374 \text{ V vs NHE} \qquad [5]$$

The contribution of these two counteranions to the pH increase was then examined by using an Ar-bubbled aqueous DMAB solution. Figure 4 shows the pH variation after the immersion of a Pd-catalyzed glass substrate into an Ar-bubbled aqueous 0.02 M DMAB solution containing 0.12 M $NaNO_3$ or $NaClO_4$. The pH variations for sodium salt-free Ar-bubbled DMAB solutions with and without the Pd-catalyzed glass substrate are examined for comparison, and the results are also plotted in Fig. 4. A time-dependent pH increase was found in each case, while the increment was much smaller than that observed in the presence of dissolved oxygen (see Fig. 2a). The apparent generation rate of OH^- calculated from the pH variation is listed in Table I. Although the pH increments are generally small in the Ar-bubbled solutions, it is important that $NaNO_3$ solution showed the largest pH-increase rate (0.21 μmol min^{-1}) among the four conditions in Fig. 4. In contrast, the pH-increase rate of $NaClO_4$ solution (0.15 μmol min^{-1}) was almost the same as that for the sodium salt-free, suggesting that ClO_4^- ions have, contrary to the expectation, a poor ability to generate OH^- ions, even though the ClO_4^-/ClO_3^- pair has a nobler redox potential ($E^0 = 0.374$ V vs NHE) than NO_3^-/NO_2^- redox pair ($E^0 = 0.01$ V). This is probably because the reduction of ClO_4^- is kinetically hindered, just as SO_4^{2-} ions are virtually stable in aqueous solutions in spite of the noble redox potential of the SO_4^-/S^- pair.[26] Similar results regarding ClO_4^- ions have also been reported for the electrodeposition of metal oxides.[27] Note that a pH increase with the apparent OH^- generation rate of 0.085 μmol min^{-1} was also recognized without the immersion of the Pd-catalyzed glass substrate. This indicates that a spontaneous decomposition of DMAB gradually takes place without the catalysis. Figure 3b shows XRD patterns for the Pd-catalyzed glass substrate after immersing in an Ar-bubbled aqueous 0.02 M DMAB solution containing 0.06 M $Zn(NO_3)_2$ or $Zn(ClO_4)_2$ for 1 h at 338 K. Wurtzite ZnO was deposited from the Ar-bubbled $Zn(NO_3)_2$ solution even with the quite low pH-increase rate. In contrast, no peak for ZnO was observed for the $ZnClO_4$ solution, demonstrating that the deposition does not take place. From the above results, it was revealed that $Zn(NO_3)_2$ is the only salt that provides ZnO independently without DO.

Effect of DO on pH increase.— The influence of DO, which accelerates the pH increase, on the chemical ZnO deposition was examined by preparing an O_2-, air-, or Ar-bubbled aqueous 0.06 M $Zn(NO_3)_2$–0.02 M DMAB solution. The concentrations of DO in these three solutions are ~1.25 mM (O_2), ~0.28 mM (air), and ~0 (Ar) at room temperature.[e] Figure 5 shows the pH variation of the solutions after the immersion of a Pd-catalyzed glass substrate at 298 K with magnetic stirring. As expected, the order of the pH-increase rate depended on the DO concentration, $O_2 >$ air $>$ Ar. As an independent experiment, ZnO films were deposited on the Pd-catalyzed glass substrate from each aqueous 0.06 M $Zn(NO_3)_2$–0.02 M DMAB solution at 338 K. The concentration of DO at 338 K can be estimated from the Bunsen absorption coefficients to be ~0.83 mM (O_2) and ~0.13 mM (air).[28] Figure 6 shows the thickness variation of ZnO obtained from the three solutions as a function of deposition time. All the curves showed rapid growth within the first 10 min [deposition rates in nanometers per minute were 14.3 (O_2), 12.4 (air), and 10.1 (Ar)], followed by gradual increases in thickness toward 3 h. Corresponding top- and tilted-

[e] The DO concentration under air- and Ar-bubbling conditions was measured with a conventional DO meter (HORIBA 9520-10D), and under O_2-bubbling was the saturation value at 298 K.

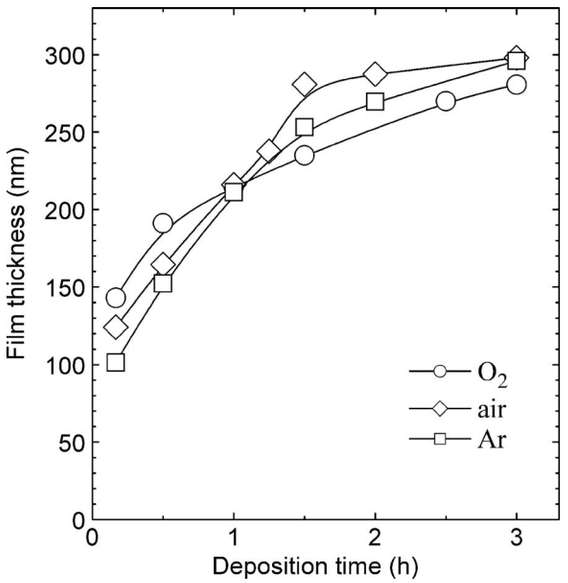

Figure 6. ZnO film thickness as a function of deposition time. The ZnO was deposited on Pd-catalyzed glass from an aqueous 0.06 M $Zn(NO_3)_2$–0.02 M DMAB solution bubbled with O_2 (○), air (◇), or Ar (□) gas.

view FESEM images of the glass substrates after 1 and 10 min deposition are depicted in Fig. 7, revealing that each substrate was almost covered with ZnO grains within 1 min. Arbitrary grains with large voids were observed for the ZnO from the O_2 or air-bubbled solution, while rather homogeneous and compact ZnO grains grew from the Ar-bubbled solution. These results indicate that ZnO grows at a remarkable rate on the order of O_2 > air > Ar until it covers the virgin Pd-catalyzed glass surface and, after that, the growth on the ZnO surface becomes moderate but continuously proceeds. Furthermore, the rapid growth caused by DO results in defective crystal nuclei probably including some $Zn(OH)_x$ due to imperfect dehydration.

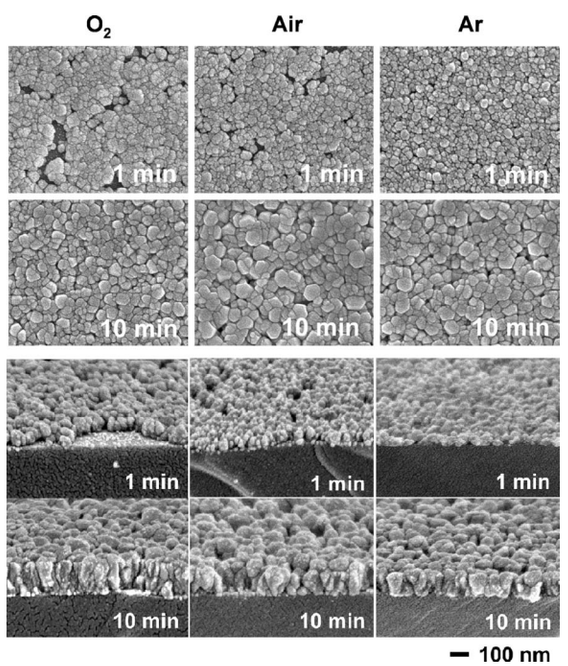

Figure 7. Top-view and tilted-view FESEM images of ZnO deposited on Pd-catalyzed glass for 1 and 10 min at 338 K from an aqueous 0.06 M $Zn(NO_3)_2$–0.02 M DMAB solution bubbled with O_2, air, or Ar gas.

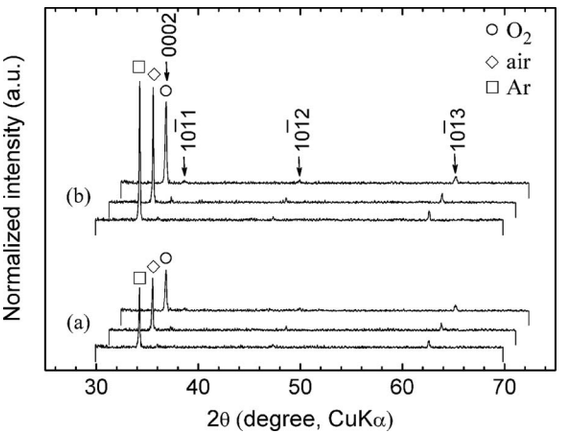

Figure 8. Normalized XRD patterns of ZnO films deposited on Pd-catalyzed glass for (a) 1 and (b) 3 h at 338 K from an aqueous 0.06 M $Zn(NO_3)_2$–0.02 M DMAB solution bubbled with O_2 (○), air (◇), or Ar (□) gas.

In the course of the chemical ZnO deposition, slight bath decomposition, (i.e., precipitation of ZnO in the bulk solution) was observed at ~2 h or later, and the growth of ZnO concomitantly slowed down. Although the initial order of the thickness (O_2 > air > Ar) depended on the DO concentration, the thickness order became air > Ar > O_2 after 2 h deposition, suggesting less influence of DO on the ZnO growth on the ZnO surface and an increase in the relative contribution of NO_3^- in the deposition process. The chemical ZnO growth on a ZnO surface was investigated by immersing a ZnO-coated glass substrate into three 0.06 M $Zn(NO_3)_2$–0.02 M DMAB solutions each treated with the following conditions: (*i*) O_2-, (*ii*) Ar-, and (*iii*) Ar-bubbling with additive 0.12 M $NaNO_3$. The ZnO-coated glass employed was preprepared by immersing a Pd-catalyzed glass substrate into an air-bubbled 0.06 M $Zn(NO_3)_2$–0.02 M DMAB solution at 338 K for 1 h. The increased thicknesses of the ZnO resulting from 2 h deposition in the above three solutions were (*i*) 119, (*ii*) 100, and (*iii*) 107 nm, corresponding to the deposition rates of (*i*) 0.99, (*ii*) 0.83, and (*iii*) 0.89 nm min^{-1}, respectively. These values are <1/10 of those for the initial 10 min deposition on the Pd-catalyzed glass substrate, and it turned out that the neither DO nor additional NO_3^- ions (as $NaNO_3$) had a remarkable effect on the ZnO growth here. These findings may well be attributed to the difference in catalytic activity and concomitant rate-determining step of the chemical redox reactions (Reactions 2-4) between on the Pd catalyst and on the ZnO surface; the reduction of DO and NO_3^- is the rate-determining step on the Pd catalyst, while the further growth of ZnO on the ZnO surface is limited by the oxidation of DMAB because the ZnO surface has less catalytic activity toward it.

Effect of dissolved oxygen on ZnO growth.— Although wurtzite ZnO generally exhibits a spontaneous *c*-axis preferred growth orientation since the (0001) basal plane has a higher surface energy, the difference in the initial nucleation process can affect the subsequent ZnO growth regime. This was investigated by XRD measurements. Figure 8 shows XRD patterns of ZnO films obtained from 1 and 3 h deposition in an aqueous 0.06 M $Zn(NO_3)_2$–0.02 M DMAB solution bubbled with O_2, air, or Ar gas. The intensity of XRD patterns was normalized in terms of film thickness for ease of comparison between the bubbling gases. Although all ZnO films had a ⟨0001⟩ preferred growth orientation, the Ar-bubbled solution gave a superior ⟨0001⟩ orientation. Independent of the bubbling gases, the in-

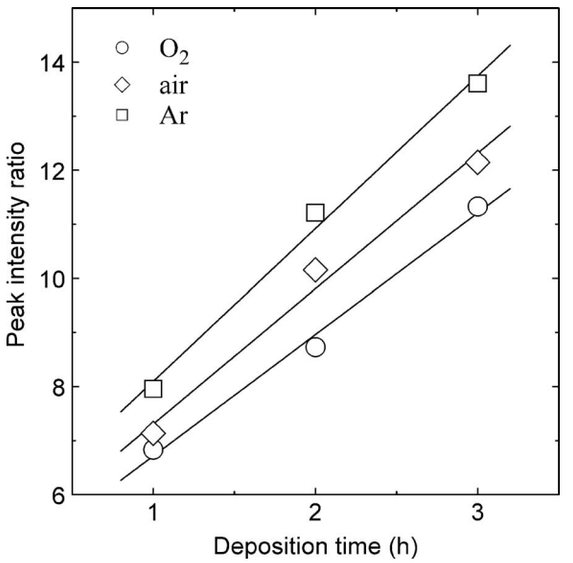

Figure 9. XRD peak intensity ratio of 0002 to $10\bar{1}3$ diffraction for the ZnO films deposited for 1–3 h at 338 K from an aqueous 0.06 M $Zn(NO_3)_2$–0.02 M DMAB solution bubbled with O_2 (○), air (◇), or Ar (□) gas.

tensity of 0002 diffraction increased with increasing deposition time, while other diffraction peaks such as $10\bar{1}3$ showed little dependence on the deposition time. This indicates that the initial growth (i.e., nucleation) on the Pd catalyst involves some randomly oriented ZnO and then *c*-axis growth progresses exclusively on the initial ZnO surface. Such phenomena can be attributed to the rapid nucleation on the Pd catalyst and the moderate growth, near the chemical equilibrium, on the ZnO surface. The variation of peak intensity ratio of 0002 to $10\bar{1}3$ for each bubbling gas was plotted against deposition time (Fig. 9), representing a linear relationship between them with inclinations of 2.8, 2.5, and 2.3 for the Ar-, air-, and O_2-bubbled solutions, respectively. The linearity implies that *c*-axis growth on the ZnO (0001) plane proceeds with a constant rate determined by the DMAB oxidation reaction (Reaction 4), and the difference in the inclination reflects the degree of *c*-axis preferred orientation. The nucleation process also affected the resulting crystallite size; the averaged values of full width at half-maximum (fwhm) of the 0002 diffraction for the 1–3 h deposition ZnO are 0.10° (Ar), 0.10° (air), and 0.14° (O_2), representing that the ZnO from the O_2-bubbled solution has a smaller crystallite size.

The presence of DO also affected the surface morphology of the ZnO films as shown in Fig. 10. After the nucleation on the Pd catalyst, columnar grains grew almost vertically to the substrate surface accompanied by the lateral growth to form a polycrystalline film (see also Fig. 7). The diameter of ZnO grains from the O_2-bubbled solution was smaller than that from the air- or Ar-bubbled solution, and the ZnO films deposited from the O_2- or air-bubbled solution have distinct gaps between the ZnO columnar grains in contrast to that from the Ar-bubbled solution. It can therefore be concluded that the nucleation process depending on the DO concentration affects the subsequent crystal growth regime including crystallinity, orientation, and surface morphology.

Effect of dissolved oxygen on the optical and electrical properties of ZnO.— Visible transparency and bandgap energy were evaluated on 240 nm thick ZnO films deposited from the three different solutions by the same method as mentioned above (Fig. 11). The spectra were taken with respect to air and hence involve contribution from a Corning glass as well as ZnO films deposited on both its sides. All the ZnO films exhibited high visible transparency of

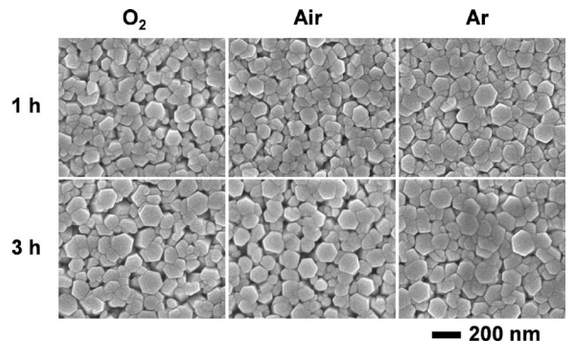

Figure 10. Top-view FESEM images of ZnO deposited on Pd-catalyzed glass for 1 and 3 h at 338 K from an aqueous 0.06 M $Zn(NO_3)_2$–0.02 M DMAB solution bubbled with O_2, air, or Ar gas.

>80% and a critical absorption edge at 367.5 nm corresponding to a bandgap energy of 3.37 eV. Thus, no significant difference in optical properties was recognized among these ZnO films grown from the O_2-, air-, or Ar-bubbled solutions in the present experimental conditions.

In contrast, there was a clear difference in electrical properties. Here, the electrical property of the ZnO films obtained by 3 h deposition was investigated using a Hall coefficient analyzer. Because the as-deposited ZnO films had high resistivity of $>10^5\ \Omega$ cm due to extremely low carrier concentration, films were heat-treated at 723 K for 30 min under a 3% H_2/Ar mixed gas atmosphere in order to increase the carrier concentration. These heat-treated ZnO films showed XRD patterns with somewhat wider fwhm without peak shifts compared to those before the heating. The results are summarized in Table II. All the ZnO films exhibited n-type conductivity as expected from the following well-known carrier-generation mechanisms: (*i*) $ZnO \rightarrow Zn_i^{\bullet} + e^- + 1/2O_2$ or (*ii*) $O_O \rightarrow V_O^{\bullet} + e^- + 1/2O_2$.[29] Resistivity was drastically decreased to a measurable level by the heat-treatment, and of importance to note here is that the ZnO film obtained from the Ar-bubbled solution showed resistivity as low as $2.67 \times 10^{-2}\ \Omega$ cm, which is one-half that for the O_2-bubbled solution. The order of carrier density was Ar > O_2 ≈ air, and that of mobility was air > Ar > O_2, suggesting that the dense columnar grains and higher crystallinity of ZnO contribute to the higher carrier concentration, and larger columnar diameter contributes to higher mobility.

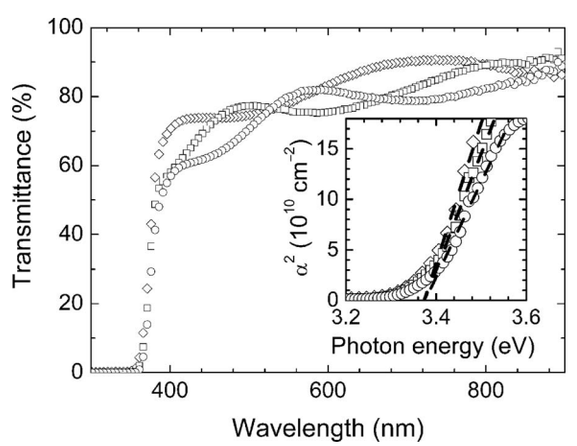

Figure 11. Transmittance spectra of 240 nm thick ZnO films deposited on Pd-catalyzed glass at 338 K from an aqueous 0.06 M $Zn(NO_3)_2$–0.02 M DMAB solution bubbled with O_2 (○), air (◇), or Ar (□) gas. Inset is dependence of α^2 (α: absorption coefficient) on photon energy.

Table II. Electrical properties for ZnO films deposited from an aqueous 0.06 M $Zn(NO_3)_2$–0.02 M DMAB solution bubbled with O_2, air, or Ar, and heat-treated at 723 K for 30 min under a 3% H_2/Ar mixed gas atmosphere.

Bubbling-gas	Resistivity (Ω cm)	Carrier density (cm^{-3})	Mobility ($cm^2\ V^{-1}\ s^{-1}$)
O_2	4.57×10^{-2}	1.22×10^{19}	11.2
Air	3.26×10^{-2}	1.21×10^{19}	15.8
Ar	2.67×10^{-2}	1.70×10^{19}	13.8

Conclusions

The effects of various counteranions (NO_3^-, Cl^-, ClO_4^-, and SO_4^{2-}) and DO on the ZnO growth regime, including a series of redox reactions in DMAB solutions, were investigated using the Pd-catalyzed glass substrate, corresponding sodium and zinc salts, and O_2, air, or Ar bubbling. Whereas the counteranions of Cl^- and SO_4^{2-} affected the Zn^{2+} hydrolysis-causing pH increase of an O_2-bubbled DMAB solution to yield zinc double salts, ZnO was obtained from the solution containing NO_3^- or ClO_4^-. Weaker interactions of a counteranion with H^+, Zn^{2+}, or Pd were suggested as an important factor for the chemical ZnO deposition, and it was found that only NO_3^- can raise the pH of a DMAB solution independently without DO. The influence of DO on the ZnO growth rate is predominant over that of NO_3^- at the initial growth on the Pd catalyst, while the influence becomes comparable to that of NO_3^- at the subsequent growth on the ZnO surface, due to the difference in their catalytic activity toward the oxidation of DMAB. The ZnO nucleation rate depending on the DO concentration affects the resultant ZnO structure in terms of crystallinity, growth orientation, and surface morphology. The control of the nucleation rate by eliminating DO in the aqueous $Zn(NO_3)_2$−DMAB solution was found to give ZnO films with higher conductivity.

T. Shinagawa assisted in meeting the publication costs of this article.

References

1. J. Koike, H. Tanaka, and H. Ieki, *Jpn. J. Appl. Phys., Part 1*, **34**, 2678 (1995).
2. M. Matsuoka, *Jpn. J. Appl. Phys.*, **10**, 736 (1971).
3. T. K. Gupta, *J. Am. Ceram. Soc.*, **73**, 1817 (1990).
4. T. Seiyama, A. Kato, K. Fujiishi, and M. Nagatani, *Anal. Chem.*, **34**, 1502 (1962).
5. T. Minami, *Semicond. Sci. Technol.*, **20**, S35 (2005), and references therein.
6. D. M. Bagnall, Y. F. Chen, Z. Zhu, T. Yao, S. Koyama, M. Y. Shen, and T. Goto, *Appl. Phys. Lett.*, **70**, 2230 (1997).
7. M. H. Huang, S. Mao, H. Feick, H. Yan, Y. Wu, H. Kind, E. Weber, R. Russo, and P. Yang, *Science*, **292**, 1897 (2001).
8. M. Izaki, S. Watase, and H. Takahashi, *Adv. Mater. (Weinheim, Ger.)*, **15**, 2000 (2003).
9. M. Izaki and T. Omi, *Appl. Phys. Lett.*, **68**, 2439 (1996).
10. M. Izaki and T. Omi, *J. Electrochem. Soc.*, **143**, L53 (1996).
11. M. Izaki and T. Omi, *J. Electrochem. Soc.*, **144**, 1949 (1997).
12. S. Peulon and D. Lincot, *Adv. Mater. (Weinheim, Ger.)*, **8**, 166 (1996).
13. S. Peulon and D. Lincot, *J. Electrochem. Soc.*, **145**, 864 (1998).
14. M. Pourbaix, *Atlas of Electrochemical Equilibtia in Aqueous Solutions*, p. 409, NACE, Houston, TX (1974).
15. M. Izaki and T. Omi, *J. Electrochem. Soc.*, **144**, L3 (1997).
16. M. Izaki and J. Katayama, *J. Electrochem. Soc.*, **147**, 210 (2000).
17. R. M. Smith and A. E. Martell, *Critical Stability Constants*, Vol. 4, Plenum Press, New York (1989).
18. R. M. Smith and A. E. Martell, *Critical Stability Constants*, Vol. 2, Plenum Press, New York (1989).
19. M. Schlesinger, in *Modern Electroplating*, 4th ed., M. Schlesinger and M. Paunovic, Editors, p. 618, Wiley Interscience, New York (2000).
20. K. Murase, H. Tada, T. Shinagawa, M. Izaki, and Y. Awakura, *J. Electrochem. Soc.*, **153**, C735 (2006).
21. J. Elias, R. Tena-Zaera, and C. Lévy-Clément, *J. Phys. Chem. C*, **112**, 5736 (2008).
22. A. Goux, T. Pauporte, J. Chivot, and D. Lincot, *Electrochim. Acta*, **50**, 2239 (2005).
23. E. Högfeldt, *Stability Constants of Metal-Ion Complexes, Part A*, Pergamon Press, Oxford (1982).
24. L.-J. Wan, T. Suzuki, K. Sashikata, J. Okada, J. Inukai, and K. Itaya, *J. Electroanal. Chem.*, **484**, 189 (2000).
25. M. A. Aramendía, V. Boráu, I. M. García, C. Jiménez, F. Lafont, A. Marinas, J. M. Marinas, and F. J. Urbano, *J. Mol. Catal. A: Chem.*, **184**, 237 (2002).
26. M. Pourbaix, *Atlas of Electrochemical Equilibtia in Aqueous Solutions*, p. 511, NACE, Houston, TX (1974).
27. G. H. A. Therese and P. V. Kamath, *Chem. Mater.*, **12**, 1195 (2000).
28. The Chemical Society of Japan, *Kagaku Binran Kisohen*, 3rd ed., p. II-158, Maruzen, Tokyo (1984).
29. P. Bonasewicz, W. Hirschwald, and G. Neumann, *Phys. Status Solidi A*, **97**, 593 (1986).